Quasistationary solutions of scalar fields around collapsing self-interacting boson stars

Alejandro Escorihuela-Tomàs,[1] Nicolas Sanchis-Gual,[1] Juan Carlos Degollado,[2] and José A. Font[1, 3]

[1]*Departamento de Astronomía y Astrofísica, Universitat de València,*
Dr. Moliner 50, 46100, Burjassot (València), Spain
[2] *Instituto de Ciencias Físicas, Universidad Nacional Autónoma de México,*
Apdo. Postal 48-3, 62251, Cuernavaca, Morelos, México.
[3]*Observatori Astronòmic, Universitat de València,*
C/ Catedrático José Beltrán 2, 46980, Paterna (València), Spain

(Dated: April 27, 2017)

There is increasing numerical evidence that scalar fields can form long-lived quasi-bound states around black holes. Recent perturbative and numerical relativity calculations have provided further confirmation in a variety of physical systems, including both static and accreting black holes, and collapsing fermionic stars. In this work we investigate this issue yet again in the context of gravitationally unstable boson stars leading to black hole formation. We build a large sample of spherically symmetric initial models, both stable and unstable, incorporating a self-interaction potential with a quartic term. The three different outcomes of unstable models, namely migration to the stable branch, total dispersion, and collapse to a black hole, are also present for self-interacting boson stars. Our simulations show that for black-hole-forming models, a scalar-field remnant is found outside the black-hole horizon, oscillating at a different frequency than that of the original boson star. This result is in good agreement with recent spherically symmetric simulations of unstable Proca stars collapsing to black holes [1].

I. INTRODUCTION

The development of stable numerical relativity codes based on hyperbolic formulations of Einstein's equations, accompanied with suitable gauge conditions, has been critical for recent advances in our understanding of astrophysical systems involving strong gravity. In particular, those technical developments have allowed accurate numerical evolutions of highly dynamical spacetimes up to, and well beyond, the formation of black holes. Further steps have also been taken with the incorporation of matter content in black-hole spacetimes, specifically in the form of scalar fields, a type of matter that has found recurrent use in numerical relativity. Within such a framework, recent studies of the Einstein-Klein-Gordon (EKG) system, both in the linear and nonlinear regime, have shown that massive scalar fields surrounding black holes can accommodate a type of oscillatory mode which only decays at infinity [2–8]. These quasi-bound states may thus linger around the black hole in the form of a long-lived remnant (a *wig*) of scalar field. For both, scalar fields around supermassive black holes and axion-like scalar fields around primordial black holes, it has been found that the fields can indeed survive for cosmological timescales [4]. Moreover, for spinning black holes, quasi-bound states can yield exponentially growing modes [9, 10] and hairy-black-hole solutions [11].

On the other hand, scalar fields are also known to allow for soliton-like solutions, i.e. static, spherically symmetric solutions of the EKG system for a massive and complex field [12, 13], which are commonly known as boson stars (see [14] for a review). The dynamical fate of boson stars has been thoroughly investigated numerically, both using perturbation theory [15, 16] and fully nonlinear numerical simulations [17–20]. Ref. [17] in particular first showed that the fate of unstable boson-star solutions was either the formation of a black hole or the migration of the star to the stable branch, regardless of the sign of the binding energy. A third outcome for unstable boson stars is their total dispersion [18, 20, 21] a situation which only happens for boson stars with negative binding energy.

In this work we build a comprehensive sample of initial models of boson stars, incorporating a self-interaction potential with a quartic term. The inclusion of such self-interaction provides extra pressure support against gravitational collapse and increases the range of possible maximum masses of boson stars, allowing to encompass models with astrophysical significance. Here, we revisit the stability of the solutions for different values of the self-interaction coupling constant λ, incorporating values as large as $\Lambda \equiv \lambda/4\pi G\mu^2 = 100$, not previously accounted for (here μ is the bare mass of the scalar field). Our findings are consistent with the three different outcomes for unstable models, namely migration to the stable branch, total dispersion, and collapse to a black hole, reported previously for both the $\lambda = 0$ (mini-)boson star case and for self-interacting boson stars (see [17, 18, 20]).

We, however, focus on a particular subset of collapsing models. Making use of the specific techniques developed by [22] to evolve black-hole spacetimes in spherical symmetry using spherical-polar coordinates, we are able to follow the dynamics of the system for very long periods of time, well beyond black hole formation and in an entirely stable manner. Using these techniques we showed recently that quasi-bound states can form in the vicinity of a black hole born dynamically from the collapse

of a neutron star surrounded by a scalar field [23]. Here we show that long-lived quasi-bound states can also form after the collapse of a self-interacting boson star. Similar results have also recently been obtained in spherical simulations of unstable Proca stars collapsing to black holes [1] as well as for axion stars [24].

This paper is organized as follows: Section II briefly describes the mathematical formulation of the EKG system. Section III discusses the construction of the initial data while Section IV gives a brief account of numerical aspects of the simulations. Our main findings and results are discussed in Section V. Finally, Section VI summarizes our conclusions. Greek indices run over spacetime indices while Latin indices run over spatial indices only. We use geometrized units, $c = G = 1$.

II. BASIC EQUATIONS

We investigate the dynamics of a self-interacting scalar field configuration around a black hole by solving numerically the coupled EKG system

$$R_{\alpha\beta} - \frac{1}{2}g_{\alpha\beta}R = 8\pi T_{\alpha\beta} , \qquad (1)$$

with the scalar field matter content given by the stress energy tensor

$$
\begin{aligned}
T_{\alpha\beta} &= \frac{1}{2}(D_\alpha\Phi)^*(D_\beta\Phi) + \frac{1}{2}(D_\alpha\Phi)(D_\beta\Phi)^* \\
&- \frac{1}{2}g_{\alpha\beta}(D^\sigma\Phi)^*(D_\sigma\Phi) - \frac{\mu^2}{2}g_{\alpha\beta}|\Phi\Phi^*| \\
&- \frac{1}{4}\lambda\, g_{\alpha\beta}|\Phi\Phi^*|^2.
\end{aligned}
\qquad (2)
$$

We consider the following potential for the scalar field $V(\Phi^2) = \mu^2|\Phi|^2 + \frac{\lambda}{2}|\Phi|^4$, where $V_{\text{int}} := \frac{1}{4}\lambda|\Phi|^4$ is a quartic self-interaction potential with coupling λ. We also introduce the dimensionless quantity $\Lambda \equiv \lambda/4\pi\mu^2$. The scalar field obeys the Klein-Gordon equation

$$\left(\Box - \frac{dV}{d|\Phi|^2}\right)\Phi = 0 , \qquad (3)$$

where the D'Alambertian operator is defined by $\Box := (1/\sqrt{-g})\partial_\alpha(\sqrt{-g}g^{\alpha\beta}\partial_\beta)$. Φ is dimensionless and μ has dimensions of $(\text{length})^{-1}$.

In spherical symmetry, the spatial line element can be written as

$$dl^2 = e^{4\chi}(a(t,r)dr^2 + r^2 b(t,r)d\Omega^2) , \qquad (4)$$

where $d\Omega^2 = d\theta^2 + \sin^2\theta d\varphi^2$ is the solid angle element and $a(t,r)$ and $b(t,r)$ are two non-vanishing metric functions. Moreover, χ is related to the conformal factor ψ as $\psi = e^\chi = (\gamma/\hat\gamma)^{1/12}$, with γ and $\hat\gamma$ being the determinants of the physical and conformal 3-metrics, respectively. They are conformally related by $\gamma_{ij} = e^{4\chi}\hat\gamma_{ij}$.

In this work we employ the Baumgarte-Shapiro-Shibata-Nakamura (BSSN) formalism of Einstein's equations [25, 26] where the evolved fields are the conformally related 3-dimensional metric, the conformal exponent χ, the trace of the extrinsic curvature K, the independent component of the traceless part of the conformal extrinsic curvature, $A_a \equiv A^r{}_r, A_b \equiv A^\theta{}_\theta = A^\varphi{}_\varphi$, and the radial component of the conformal connection functions. The interested reader is addressed to [6, 27, 28] for further details. In particular, the explicit form of the evolution equations for the gravitational field that we use in this work are given by Eqs. (9)-(11) and (13)-(15) in Ref. [6].

As in our previous work [29], in order to solve the Klein-Gordon equation we use two first-order variables defined as

$$\Pi := n^\alpha\partial_\alpha\Phi = \frac{1}{\alpha}(\partial_t\Phi - \beta^r\partial_r\Phi) , \qquad (5)$$

$$\Psi := \partial_r\Phi . \qquad (6)$$

Therefore, from Eq. (3) we obtain the following system of first-order equations:

$$\partial_t\Phi = \beta^r\partial_r\Phi + \alpha\Pi , \qquad (7)$$

$$\partial_t\Psi = \beta^r\partial_r\Psi + \Psi\partial_r\beta^r + \partial_r(\alpha\Pi) , \qquad (8)$$

$$
\begin{aligned}
\partial_t\Pi &= \beta^r\partial_r\Pi + \frac{\alpha}{ae^{4\chi}}\Big[\partial_r\Psi \\
&+ \Psi\left(\frac{2}{r} - \frac{\partial_r a}{2a} + \frac{\partial_r b}{b} + 2\partial_r\chi\right)\Big] \\
&+ \frac{\Psi}{ae^{4\chi}}\partial_r\alpha + \alpha K\Pi - \alpha(\mu^2 + \lambda\Phi^2)\Phi .
\end{aligned}
\qquad (9)
$$

The right-hand-sides of the gravitational field evolution equations contain matter source terms (see Eqs. (9)-(11) and (13)-(15) in [6]), denoted by $\mathcal{E}$, S_a, S_b and j_r. These terms are components of the energy-momentum tensor, Eq. (2), or suitable projections thereof, and are given by

$$
\begin{aligned}
\mathcal{E} &:= n^\alpha n^\beta T_{\alpha\beta} = \frac{1}{2}\left(|\Pi|^2 + \frac{|\Psi|^2}{ae^{4\chi}}\right) \\
&+ \frac{1}{2}\mu^2|\Phi|^2 + \frac{1}{4}\lambda|\Phi|^4,
\end{aligned}
\qquad (10)
$$

$$j_r := -\gamma^\alpha_r n^\beta T_{\alpha\beta} = -\frac{1}{2}\left(\Pi^*\Psi + \Psi^*\Pi\right) , \qquad (11)$$

$$
\begin{aligned}
S_a &:= T^r_r = \frac{1}{2}\left(|\Pi|^2 + \frac{|\Psi|^2}{ae^{4\chi}}\right) \\
&- \frac{1}{2}\mu^2|\Phi|^2 - \frac{1}{4}\lambda|\Phi|^4 ,
\end{aligned}
\qquad (12)
$$

$$
\begin{aligned}
S_b &:= T^\theta_\theta = \frac{1}{2}\left(|\Pi|^2 - \frac{|\Psi|^2}{ae^{4\chi}}\right) \\
&- \frac{1}{2}\mu^2|\Phi|^2 - \frac{1}{4}\lambda|\Phi|^4 .
\end{aligned}
\qquad (13)
$$

The Hamiltonian and momentum constrains are given

by the following two equations:

$$\mathcal{H} \equiv R - (A_a^2 + 2A_b^2) + \frac{2}{3}K^2 - 16\pi\mathcal{E} = 0, \quad (14)$$

$$\mathcal{M}_r \equiv \partial_r A_a - \frac{2}{3}\partial_r K + 6A_a\partial_r\chi$$
$$+ (A_a - A_b)\left(\frac{2}{r} + \frac{\partial_r b}{b}\right) - 8\pi j_r = 0. \quad (15)$$

The latter two equations are only computed in our code to monitor the accuracy of the numerical evolutions.

III.   INITIAL DATA

Spherical boson stars are described by the radial function $\Phi(r,t) = \Phi_0(r)e^{i\omega t}$ where ω is the oscillation frequency of the field. Following [30] we obtain the initial data for a boson star in polar-areal coordinates, for which the line element is given by

$$ds^2 = -\alpha^2(r')dt^2 + a^2(r')dr^2 + r'^2 d\Omega^2 , \quad (16)$$

and r' is the radial coordinate. The EKG system for a boson star reads:

$$\frac{\partial_{r'}a}{a} = \frac{1-a^2}{2r'} + 2\pi r'\left[\omega^2\Phi_0^2\frac{a^2}{\alpha^2} + \Psi_0^2\right.$$
$$\left. + a^2\Phi_0^2\left(\mu^2 + \frac{1}{2}\lambda\Phi_0^2\right)\right] , \quad (17)$$

$$\frac{\partial_{r'}\alpha}{\alpha} = \frac{a^2-1}{r'}$$
$$+ \frac{\partial_{r'}a}{a} - 4\pi r'a^2\Phi_0^2\left(\mu^2 + \frac{1}{2}\lambda\Phi_0^2\right) , \quad (18)$$

$$\partial_{r'}\Phi_0 = \Psi_0 , \quad (19)$$

$$\partial_{r'}\Psi_0 = -\Psi_0\left(\frac{2}{r'} + \frac{\partial_{r'}\alpha}{\alpha} - \frac{\partial_{r'}a}{a}\right)$$
$$- \omega^2\Phi_0^2\frac{a^2}{\alpha^2} + a^2(\mu^2 + \lambda\Phi_0^2)\Phi_0 . \quad (20)$$

By solving these equations we obtain the spacetime metric potentials, $g_{tt} = -\alpha^2, g_{rr} = a^2$, and the radial distribution of the scalar field, Φ_0. The mass of a boson star is computed using the definition of the Misner-Sharp mass function,

$$M_{\text{MS}} = \frac{r'_{\text{max}}}{2}\left(1 - \frac{1}{a^2(r'_{\text{max}})}\right) , \quad (21)$$

where r'_{max} is the radial coordinate at the outer boundary of our computational grid. The total mass of a boson star can also be computed using the Komar integral [31],

$$M_{\text{BS}} = \int_\Sigma \left(2T_t^t - T_\alpha^\alpha\right)\alpha\sqrt{\gamma}\,dr\,d\theta\,d\varphi , \quad (22)$$

where Σ is a spacelike slice extending from a horizon, in case one exists, up to spatial infinity. To study the
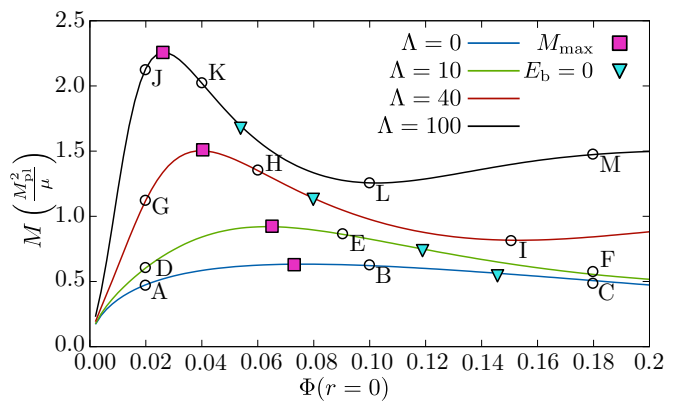

FIG. 1: Boson star mass as a function of the central value of the scalar field for a few sequences of equilibrium models with $\Lambda = \{0, 10, 40, 100\}$. For each value of Λ the purple squares indicate the maximum mass of the sequence, separating the stable and unstable branches, and the inverted cyan triangles indicate the point at which the binding energy is zero. The empty circles (and letters) indicate the specific models we evolve in this work.

stability properties of the constructed equilibrium models we need to compute the Noether charge associated with the total bosonic number N, which is defined as

$$N = \int g^{0\nu}j_\nu\alpha\sqrt{\gamma}\,dr\,d\theta\,d\varphi , \quad (23)$$

where $j_\nu = \frac{i}{2}(\Phi^*\partial_\nu\Phi - \Phi\partial_\nu\Phi^*)$ is the conserved current associated with the transformation of the U(1) group. Finally, the sign of the binding energy

$$E_{\text{b}} = M_{\text{MS}} - N\mu, \quad (24)$$

will determine the outcome of unstable models.

Representative sequences of equilibrium models of boson stars are plotted in Figure 1. This figure shows four different mass profiles as a function of the central scalar field value for four different values of the self-interaction coupling constant, namely $\Lambda = \{0, 10, 40, 100\}$. For any given Λ two important points are explicitly indicated in each curve, the maximum mass, marked with a purple square, and the point at which $E_{\text{b}} = 0$, marked with a cyan inverted triangle. For each sequence, the location of the maximum mass indicates the critical point separating the stable and the unstable branches. Boson stars situated at the left of the point of maximum mass are stable, while those on the right are unstable. The maximum mass increases monotically with $\Lambda^{1/2}$ [32]. For sufficiently large values of Λ the self-interaction term allows for significantly larger masses than for non-self-interacting (mini-)boson stars.

We study the stability of these equilibrium models through numerical time evolutions. These are triggered by adding suitable small-amplitude perturbations to the initial data profiles. We consider two types of perturbations, either those associated with the intrinsic truncation error of the finite-difference representation of the

TABLE I: Initial parameters for the bosons stars with $\mu = 1$. Λ is the self-interaction coupling constant, $\Phi(r = 0)$ is the central value of the scalar field, R is the radius, M_{MS} is the Misner-Sharp mass, M_{BS} is the scalar-field total mass, N is the bosonic number, E_b is the binding energy and ω is the frequency. Models A, D, G, and J are stable; models B, E, H, and K can collapse to a black hole or migrate depending on the perturbation; and models C, F, I, L, and M disperse away.

Model	Λ	$\Phi(r = 0)$	R	M_{MS}	M_{BS}	N	$E_{\mathrm{b}} = M_{\mathrm{MS}} - N\mu$	ω
A	0	0.02	68.79	0.47514	0.47517	0.48197	-0.00683	0.95394
B	0	0.10	32.00	0.62180	0.62029	0.63736	-0.01556	0.82269
C	0	0.18	28.18	0.50671	0.49702	0.47201	0.03470	0.76883
D	10	0.02	64.55	0.60425	0.60429	0.61585	-0.01160	0.94580
E	10	0.09	30.76	0.86314	0.86103	0.89092	-0.02778	0.79838
F	10	0.18	29.61	0.55419	0.53416	0.46712	0.08707	0.81866
G	40	0.02	57.72	1.12319	1.12327	1.16316	-0.03997	0.91481
H	40	0.06	30.39	1.35099	1.35036	1.40322	-0.05223	0.79616
I	40	0.15	33.13	0.81671	0.79145	0.70741	0.10930	0.86111
J	100	0.02	45.77	2.13376	2.13398	2.25789	-0.12413	0.86267
K	100	0.04	29.53	2.02134	2.02138	2.10953	-0.08819	0.79656
L	100	0.10	30.50	1.26039	1.23670	1.14872	0.11167	0.85837
M	100	0.18	30.70	1.47383	1.45448	1.38584	0.08799	0.85576

PDEs we solve or those associated with a functional modification of the actual radial distributions. While the evolutions of the boson stars may seem a priori easily predictable, telling from their location with respect to the maximum in the M_{BS} vs. $\Phi(r = 0)$ diagram, there are other aspects to consider which may affect the actual evolutions. In fact, depending on the sign of the binding energy, the point at which $E_{\mathrm{b}} = 0$, and on the perturbation, the stars will undergo different fates. On the one hand, as we show below, an unstable boson star with positive binding energy which is perturbed only with the discretization numerical error, migrates to the model with the same mass in the corresponding stable branch. However, if it is perturbed by slightly increasing its mass, it can collapse gravitationally and form a black hole. On the other hand, a boson star with an excess energy, i.e. placed at the right of the zero binding energy point, is no longer bounded and it will disperse away with time.

The specific boson-star models that we generate and evolve numerically are indicated by the empty circles in Fig. 1. Quantitative details of the main model parameters are reported in Table I. The boson star initial configurations are built in polar-areal coordinates but the time evolutions are performed in our code using isotropic coordinates, Eq. (4). To solve this problem, we have to take two steps, see [32, 33]. First, we perform a change of coordinates from polar-areal to isotropic coordinates with

$$r_{\mathrm{max}} = \left[\left(\frac{1 + \sqrt{a(r'_{\mathrm{max}})}}{2} \right)^2 \frac{r'_{\mathrm{max}}}{a(r'_{\mathrm{max}})} \right] , \quad (25)$$

$$\frac{dr}{dr'} = a\frac{r}{r'} , \quad (26)$$

where Eq. (25) is used as the initial value to integrate Eq. (26) backwards. Then, we obtain the conformal factor using

$$\psi = \sqrt{\frac{r'}{r}} . \quad (27)$$

With this procedure our initial solution is described in isotropic coordinates and we can write the initial values of the other scalar field quantities as:

$$\Phi(r, t = 0) = \Phi_0 , \quad (28)$$
$$\Psi(r, t = 0) = \Psi_0 , \quad (29)$$
$$\Pi(r, t = 0) = i\frac{\omega}{\alpha}\Phi_0 . \quad (30)$$

Finally, we interpolate the solution in an isotropic grid employing a cubic-spline interpolation [34] that guarantees the continuity of the second derivative to minimize high-frequency noise associated with the interpolation.

IV. NUMERICAL FRAMEWORK

As in our previous papers, the BSSN evolution equations for the geometry and the evolution equations for the scalar field are solved numerically using a second-order PIRK scheme [35, 36]. This scheme can handle in a satisfactory way the singular terms that appear in the evolution equations due to our choice of curvilinear coordinates. Explicit details about our numerical implementation have been reported e.g. in [29]. We also note that the convergence properties of our numerical code have been extensively tested before in various physical systems, including the EKG equations with self-interaction, see e.g. [6, 7, 29, 37].
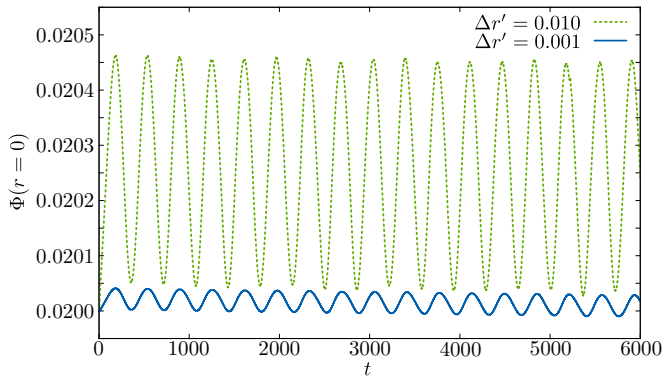
FIG. 2: Time evolution of the central value of the scalar field for boson star model A ($\Phi(r = 0, t = 0) = 0.02$ and $\Lambda = 0$) for two different resolutions of the initial data grid ($\Delta r'$).

FIG. 3: Time evolution of the central value of the scalar field for a boson star with $\Phi(r = 0, t = 0) = 0.02$ and two different values of the self-interaction coupling constant $\Lambda = \{0, 100\}$, corresponding to models A and J, respectively. The evolutions were done with the grid resolution of the initial data $\Delta r' = 0.001$.

In the simulations reported in this work we consider two computational grids, namely a grid to obtain the equilibrium models of boson stars in polar-areal coordinates, and another one to evolve those models in isotropic coordinates. Our polar-areal grid is an equidistant grid with spatial resolution $\Delta r' = 0.001$ spanning the interval $r' \in [0.0, 150.0]$. On the other hand, our isotropic grid is composed of two patches, a geometrical progression in the interior part up to a given radius and a hyperbolic cosine outside. Using the inner grid alone would require too many grid points to place the outer boundary sufficiently far from the origin (and hence prevent the effects of possible spurious reflections), while using only the hyperbolic cosine patch would produce very small grid spacings in the inner region of the domain, leading to prohibitively small timesteps due to the Courant-Friedrichs-Lewy (CFL) condition. Details about the computational grid can be found in [7]. In our work the minimum resolution Δr we choose for the isotropic logarithmic grid is $\Delta r = 0.025$. With this choice the inner boundary is then set to $r_{\min} = 0.0125$ and the outer boundary is placed at $r_{\max} = 6000$ at the nearest (in some models it is placed even further away, at $r_{\max} = 10000$). The time step is given by $\Delta t = 0.3 \Delta r$ in order to obtain long-term stable simulations.

V. RESULTS

A. Stable models

Models A, D, G, and J in Fig. 1 are all stable models. Therefore, the time evolution of the physical quantities that characterize them, as e.g. the central value of the scalar field, should remain constant. However, due to the grid discretization error, any of those quantities will instead oscillate around the equilibrium value. This is shown in Fig. 2 where we plot the central value of the scalar field for model A for two different resolutions of
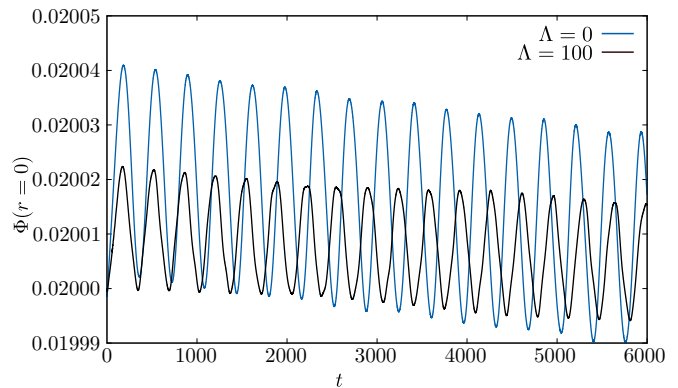
the polar-areal grid employed to build the initial data. In this figure we can also observe how when the resolution of the initial data is reduced from $\Delta r' = 0.01$ to $\Delta r' = 0.001$ the amplitude of the oscillation is significantly reduced. All of our stable initial models are indeed seen to oscillate around the central equilibrium values. As an example of their stability we plot in Fig. 3 the time evolution of the central scalar field for models A ($\Lambda = 0$) and J ($\Lambda = 100$). Note that the (purely numerical) secular drift of the initial central value of the scalar field of model A apparent in Fig. 3 and hardly visible in Fig. 2 (compare the two blue curves, both corresponding to the model with $\Lambda = 0$) is simply a consequence of the change of scale in the vertical axes of both figures. By Fourier-transforming the time evolution of the central value of the scalar field we obtain the corresponding frequency of oscillation ω of the models. Those values are reported in the last column of Table I. The stable models oscillate with a single fundamental frequency whose value decreases with increasing Λ.

B. Unstable models

Another possible outcome of the evolution of our initial data is the total dispersion of the boson star or its gravitational collapse. Let us start considering the first possibility. Such unstable situation will happen when the binding energy is positive since due to the energy excess the star will no longer remain bounded. The subset of initial models that can follow this trend are boson stars C, F, I, L, and M in Fig. 1. As an example we plot in Fig. 4 the radial profiles of the scalar field at selected times of the evolution corresponding to model C (indicated in the legend). In this case the central value of the scalar field rapidly decreases with time, the boson star suffers a drastic radial expansion and disperses away. All
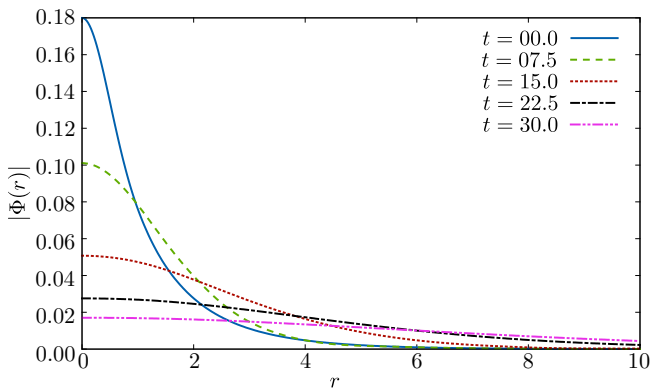
FIG. 4: Radial profile of the scalar field amplitude for different times, $t = \{0.0, 7.5, 15.0, 22.5, 30.0\}$, with $\Phi(r = 0, t = 0) = 0.18$ and $\Lambda = 0.0$ corresponding with the C case.

other unstable models (F, I, L and M) with a positive binding energy display the same fate.

Let us now consider the evolution of initial models that are located in the unstable branch, i.e. between the critical point (maximum mass of the configuration) and the $E_{\mathrm{b}} = 0$ point. These are models B, E, H, and K in Fig. 1. Previous numerical work [21] has shown that the fate of these models is to collapse gravitationally to form a black hole. However, we find that these models can also *migrate* to the stable branch of equilibrium configurations, depending on the perturbation (see also earlier work by [17]). If the only perturbation of the initial data is the one due to the discretization error, the outcome is a migration to the stable branch. However, if we include a slightly larger perturbation in the initial data, the models collapse to form black holes. The first type of evolution, while mathematically plausible but unlikely on physical grounds, has been previously observed in the case of neutron stars (see [38] for details and arguments against this evolution), boson stars [17] and, recently, also in the case of unstable Proca stars [1]. A migrating boson star will result in a different boson star. It will have the same mass but it will be located in the stable branch of the equilibrium configurations (and hence the central scalar field will have a smaller value). As an example, Fig. 5 shows the migration of boson star models E and K. For model E the star moves from a central value of the scalar field $\Phi(r = 0, t = 0) = 0.09$ towards a final value of $\Phi(r = 0) \sim 0.04$. This is precisely the value for which we obtain a stable boson star with the same mass (cf. Fig. 1). In the bottom panel of Fig. 5 one can also observe that, besides the overall migration, the evolution of model K excites more frequencies of oscillation than that of model E. This behaviour is consistent with the fact that the nonlinear term in the potential induces nonlinear couplings among the frequencies, which are more apparent the larger the value of the self-interaction coupling constant.

Let us now consider the evolution of truly perturbed unstable models. To perturb these models we add an ex-
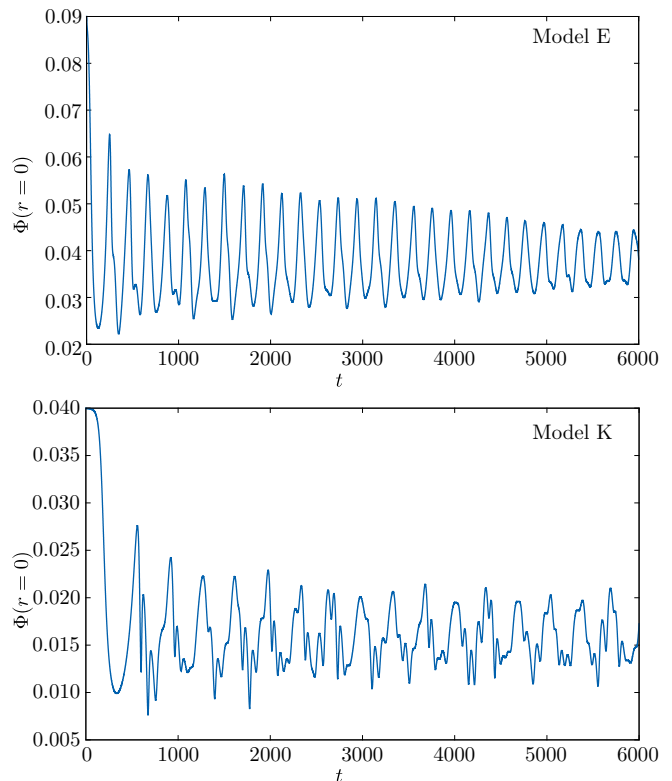

FIG. 5: Time evolution of the central value of the scalar field for the non-perturbed unstable boson star models E ($\Lambda = 10$; top panel) and K ($\Lambda = 100$; bottom panel). The stars migrate to the stable branch and oscillate around the value corresponding to models with the same mass.

tra 2% value to the initial scalar field by multiplying Φ by 1.02 after solving equations (17)-(20). We have checked by computing the binding energy that the perturbation does not change the sign. We then compute the auxiliary variables given by Eqs. (28)-(30) using the perturbed scalar field. For simplicity, after adding the perturbation we do not recompute the spacetime variables a and α. This produces a slight violation of the constraints and leads to a small difference between the masses computed with Eq. (22) and Eq. (21) in polar-areal coordinates. However, since the perturbation is fairly small (yet still larger than that associated with the discretization error) it does not substantially alter our original solution.

To diagnose the appearance of a black hole in the evolution we compute the mass of the BH through the apparent horizon (AH) area $\mathcal{A}$, using $M_{\mathrm{BH}} = \sqrt{\mathcal{A}/16\pi}$. The time evolution of both the scalar field energy (mass) and the BH mass for all unstable models is shown in Fig. 6. The mass of the boson star is computed using the Komar integral, Eq. (22). Contrary to the migrating case, adding a 2% perturbation on the initial data triggers the collapse of the solutions and at some point in the evolution an AH forms. This time is indicated in Fig. 6 by the sudden change that is observed in the evolution of the energy of the scalar field, which is associated with the
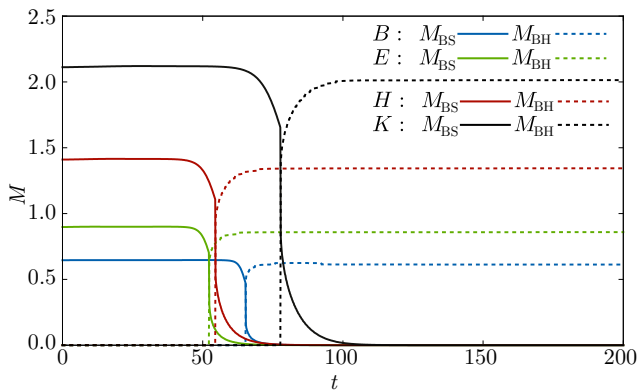
FIG. 6: Time evolution of the scalar field mass/energy (continuous lines) and the BH mass (dashed lines) for the four different unstable models B, E, H and K after the introduction of a 2% perturbation in the initial data.

sudden increase of the black hole mass from a zero value.

Fig. 6 shows that, as expected, there is a small difference between the boson star masses computed with Eq. (22) and the black hole masses computed through the apparent horizon. This is because some part of the scalar field is released after the collapse. For all models, the black hole mass is consistently, and slightly, smaller (see Table II). This means that during the collapse to a black hole, a remnant of the initial scalar field is not swallowed by the hole but instead lingers around in the form of a spherical shell or cloud. Figs. 7 and 8 show the time evolution of the amplitude of the central value of the scalar potential for the four unstable models. This time series is extracted at an observation point with a fixed radius $r_{\rm obs} = 10$. The scalar field does not disappear after the formation of the AH (which takes place for all models (well) before $t = 100$; cf. Fig. 6), forming instead long-lived quasi-bound states. For all of the models the field is seen to be clearly oscillating, as it is best visualized in the insets of the two figures. To identify the frequencies at which the field oscillates we perform a Fourier transform of the time series and obtain the power spectrum. This power spectrum shows a set of distinct frequencies, as indicated in Table II. Moreover, models B, E, and H, show a distinctive beating pattern due to the presence of overtones of the fundamental frequency.

In order to compare the frequencies of the scalar clouds resulting from the collapse of boson stars with the known frequencies of quasi-bound states around Schwarzschild black holes, we consider next a scenario in which initially the black hole is already formed and has the same mass than that formed after the collapse of a boson star. This initial Schwarzschild black hole is surrounded by a Gaussian spherical shell of scalar field which is evolved maintaining the background metric fixed. In this setup we find that after a short initial transient the field settles down into a long-lived mode akin to the ones showed in Figs. 7 and 8. In order to characterize this field we
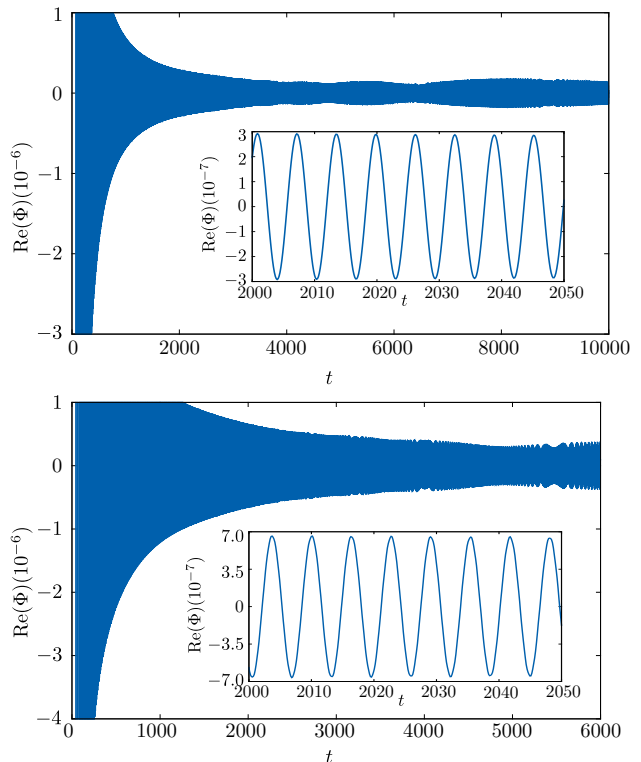

FIG. 7: Time evolution of the real part of the central value of the scalar field for the perturbed boson star models B (top panel) and E (bottom panel). The insets show a magnified view of $t \in [2000, 2050]$ in the evolution to highlight the oscillatory behaviour of the scalar field that lingers outside of the black hole.

TABLE II: Masses of unperturbed boson stars, $M_{\rm BS}$, masses of the black holes formed following boson star collapse, $M_{\rm BH}$, and frequencies of the scalar-field quasi-bound states, either computed after black hole formation, $\omega_{\rm qb}^{(1)}$, or computed from the scattering of a Gaussian pulse, $\omega_{\rm qb}^{(2)}$.

Model	Λ	$\Phi(r=0)$	$M_{\rm BS}$	$M_{\rm BH}$	$\omega_{\rm qb}^{(1)}$	$\omega_{\rm qb}^{(2)}$
B	0	0.10	0.62029	0.61271	0.99573	0.99574
E	10	0.09	0.86103	0.85875	0.99274	0.99274
H	40	0.06	1.35036	1.34378	0.98960	0.98960
K	100	0.04	2.02138	2.01382	0.98541	0.98541

Fourier-transform its amplitude to obtain the oscillation frequencies $\omega_{\rm qb}^{(2)}$. The results are shown in the last column of Table II. The excellent agreement between the frequencies $\omega_{\rm qb}^{(1)}$ computed after black hole formation and the frequencies $\omega_{\rm qb}^{(2)}$ computed from the Gaussian pulse, is a clear indication that the configurations formed after the collapse of boson stars are indeed nonlinear quasi-bound states.

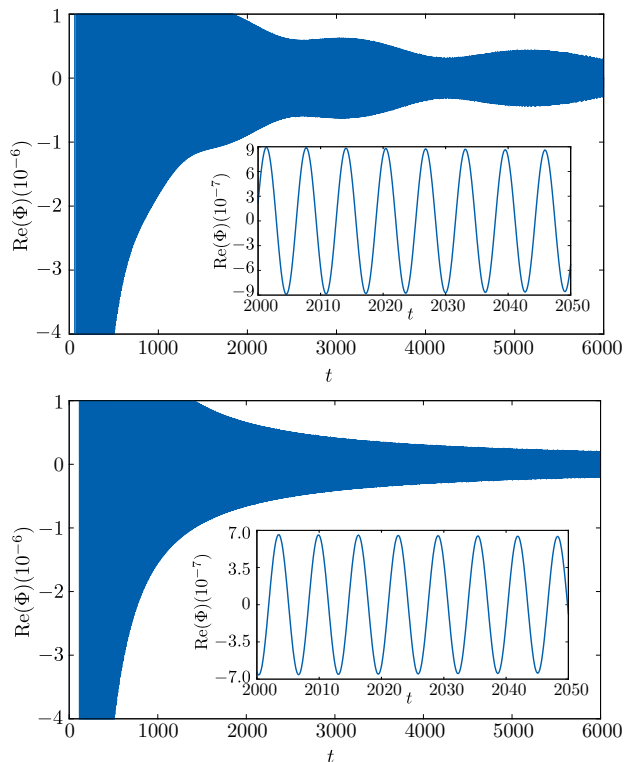Finally, in order to study the effect of Λ on the frequencies and on the time decay of the quasi-bound states,

FIG. 8: Same as Fig. 7 but for models H (top panel) and K (bottom panel).

we perform the same scattering experiment but keeping the mass $M_{\rm BH}$ fixed. We find that for sufficiently long times $t \sim 10^5 M_{\rm BH}$ the effect of Λ on the scalar field becomes negligible. This result is expected because the field decays exponentially and the dominating term is the the scalar-field mass. Therefore, despite the presence of nonlinear terms in the potential, the frequencies of all quasi-bound states will eventually tend to that of the quasi-bound state with $\Lambda = 0$ (for the same black hole mass). The timescale to reach that situation depends on the value of Λ because the frequency is different for each value of the coupling constant (both, the real and imaginary parts). Note that if we rescale the frequencies reported in Table II with the BH mass, they do not coincide.

VI. CONCLUSIONS

We have presented a new numerical study of the Einstein-Klein-Gordon system in spherical symmetry. In particular we have discussed numerical relativity simulations of a large number of initial models of boson stars, both stable and unstable, and which incorporate a self-interaction potential with a quartic term. Self-interaction provides extra pressure support against gravitational collapse, increasing the range of possible maximum masses of boson stars, allowing to encompass models with possibly larger astrophysical significance. We have revisited the stability of the initial solutions for different values of the self-interaction coupling constant Λ, as large as $\Lambda = 100$, not previously considered in the literature (to the best of our knowledge). Our simulations have shown that the three different outcomes for unstable models, namely migration to the stable branch, total dispersion, and collapse to a black hole, reported before for the $\Lambda = 0$ (mini-)boson star case [17, 18, 20], are also present for self-interacting boson stars. We have focused our investigation on a subset of collapsing models, studying the effects the self-interaction potential may have in the presence of quasi-bound states. The existence of such long-lived quasi-bound states around black holes is supported by increasing numerical evidence, both based on perturbative calculations as on fully numerical relativity [2–8]. Moreover, they have been confirmed in a variety of physical systems, including both static and accreting black holes, and collapsing fermionic stars. In this work we have revisited this issue in the context of gravitationally unstable boson stars leading to black hole formation. We have found that for black-hole-forming models, a scalar field remnant can indeed be found outside the black hole horizon, oscillating at a different frequency than that of the original boson star. This result is in good agreement with recent spherically symmetric simulations of unstable Proca stars collapsing to black holes [1].

[1] N. Sanchis-Gual, C. Herdeiro, E. Radu, J. C. Degollado, and J. A. Font, arXiv preprint arXiv:1702.04532 (2017).

[2] H. Witek, V. Cardoso, A. Ishibashi, and U. Sperhake, Phys.Rev. **D87**, 043513 (2013), 1212.0551.

[3] J. Barranco, A. Bernal, J. C. Degollado, A. Diez-Tejedor, M. Megevand, et al., Phys.Rev. **D84**, 083008 (2011), 1108.0931.

[4] J. Barranco, A. Bernal, J. C. Degollado, A. Diez-Tejedor, M. Megevand, et al., Phys.Rev.Lett. **109**, 081102 (2012), 1207.2153.

[5] J. Barranco, A. Bernal, J. C. Degollado, A. Diez-Tejedor, M. Megevand, et al., Phys.Rev. **D89**, 083006 (2014), 1312.5808.

[6] N. Sanchis-Gual, J. C. Degollado, P. J. Montero, and J. A. Font, Physical Review D **91**, 043005 (2015).

[7] N. Sanchis-Gual, J. C. Degollado, P. J. Montero, J. A. Font, and V. Mewes, Physical Review D **92**, 083001 (2015).

[8] N. Sanchis-Gual, J. C. Degollado, P. Izquierdo, J. A. Font, and P. J. Montero, Phys. Rev. D **94**, 043004 (2016), 1606.05146.

[9] S. L. Detweiler, Phys.Rev. **D22**, 2323 (1980).

[10] S. R. Dolan, Phys.Rev. **D76**, 084001 (2007), 0705.2880.

[11] C. A. R. Herdeiro and E. Radu, Phys.Rev.Lett. **112**, 221101 (2014), 1403.2757.

[12] D. J. Kaup, Phys. Rev. **172**, 1331 (1968).

[13] R. Ruffini and S. Bonazzola, Phys. Rev. **187**, 1767 (1969).

[14] S. L. Liebling and C. Palenzuela, Living Rev. Rel. **15**, 6 (2012), 1202.5809.

[15] M. Gleiser and R. Watkins, Nucl. Phys. **B319**, 733 (1989).

[16] T. D. Lee and Y. Pang, Nucl. Phys. **B315**, 477 (1989), [,129(1988)].

[17] E. Seidel and W.-M. Suen, Phys. Rev. **D42**, 384 (1990).

[18] J. Balakrishna, E. Seidel, and W.-M. Suen, Phys. Rev. **D58**, 104004 (1998), gr-qc/9712064.

[19] S. H. Hawley and M. W. Choptuik, Phys. Rev. **D62**, 104024 (2000), gr-qc/0007039.

[20] F. S. Guzman, Phys. Rev. **D70**, 044033 (2004), gr-qc/0407054.

[21] F. Guzmán, Revista mexicana de física **55**, 321 (2009).

[22] N. Sanchis-Gual, P. J. Montero, J. A. Font, E. Mller, and T. W. Baumgarte, Phys. Rev. **D89**, 104033 (2014),

[23] N. Sanchis-Gual, J. C. Degollado, P. J. Montero, J. A. Font, and V. Mewes, Phys. Rev. **D92**, 083001 (2015), 1507.08437.

[24] T. Helfer, D. J. E. Marsh, K. Clough, M. Fairbairn, E. A. Lim, and R. Becerril, JCAP **1703**, 055 (2017), 1609.04724.

[25] T. W. Baumgarte and S. L. Shapiro, Phys. Rev. D **59**, 024007 (1998).

[26] M. Shibata and T. Nakamura, Phys. Rev. D **52**, 5428 (1995).

[27] M. Alcubierre and M. D. Mendez, Gen.Rel.Grav. **43**, 2769 (2011), 1010.4013.

[28] P. J. Montero and I. Cordero-Carrion, Phys.Rev. **D85**, 124037 (2012), 1204.5377.

[29] N. Sanchis-Gual, J. C. Degollado, C. Herdeiro, J. A. Font, and P. J. Montero, Physical Review D **94**, 044061 (2016).

[30] M. Colpi, S. L. Shapiro, and I. Wasserman, Phys. Rev. Lett. **57**, 2485 (1986).

[31] C. Herdeiro, E. Radu, and H. Rúnarsson, Classical and Quantum Gravity **33**, 154001 (2016).

[32] S. L. Liebling and C. Palenzuela, Living Rev. Relativity **15** (2012).

[33] C.-W. Lai, arXiv preprint gr-qc/0410040 (2004).

[34] W. H. Press, S. A. Teukolsky, W. T. Vetterling, and B. P. Flannery, *Numerical recipes in fortran (cambridge)* (1992).

[35] I. Cordero-Carrión and P. Cerdá-Durán, ArXiv e-prints (2012), 1211.5930.

[36] I. Cordero-Carrión and P. Cerdá-Durán, *Advances in Differential Equations and Applications*, SEMA SIMAI Springer Series Vol. 4 (Springer International Publishing Switzerland, Switzerland, 2014).

[37] N. Sanchis-Gual, J. C. Degollado, P. J. Montero, J. A. Font, and C. Herdeiro, Physical review letters **116**, 141101 (2016).

[38] J. A. Font, T. Goodale, S. Iyer, M. Miller, L. Rezzolla, E. Seidel, N. Stergioulas, W.-M. Suen, and M. Tobias, Phys. Rev. D **65**, 084024 (2002), gr-qc/0110047.

1403.3653.